



HAL
open science

Modelling and Analysis of the Geometrical Errors of a Parallel Manipulator Micro-CMM

Ali Rugbani, Kristiaan Schreve

► **To cite this version:**

Ali Rugbani, Kristiaan Schreve. Modelling and Analysis of the Geometrical Errors of a Parallel Manipulator Micro-CMM. 6th International Precision Assembly Seminar (IPAS), Feb 2012, Chamonix, France. pp.105-117, 10.1007/978-3-642-28163-1_14 . hal-01363891

HAL Id: hal-01363891

<https://inria.hal.science/hal-01363891>

Submitted on 12 Sep 2016

HAL is a multi-disciplinary open access archive for the deposit and dissemination of scientific research documents, whether they are published or not. The documents may come from teaching and research institutions in France or abroad, or from public or private research centers.

L'archive ouverte pluridisciplinaire **HAL**, est destinée au dépôt et à la diffusion de documents scientifiques de niveau recherche, publiés ou non, émanant des établissements d'enseignement et de recherche français ou étrangers, des laboratoires publics ou privés.



Distributed under a Creative Commons Attribution 4.0 International License

Modelling and Analysis of the Geometrical Errors of a Parallel Manipulator micro-CMM

Ali Rugbani, Kristiaan Schreve
Department of Mechanical and Mechatronic Engineering, Stellenbosch University,
Stellenbosch, South Africa
e-mail: {ruginani, kschreve}@sun.ac.za

Abstract. A micro coordinate measurement machine (micro-CMM) with high precision and high accuracy is introduced for the measurement of part dimensions in micro scale. This design is intended to achieve submicron resolution for a work envelop of at least (100x100x100) mm. In this study, a mathematical measuring model to explicitly define the coordinate of the probe in x , y and z directions have been represented. An algorithm to find the workspace was implemented. The error model of the machine was created and the effect of structural errors on probe position was studied analytically. The significance of each geometric parameter was studied in order to minimize the measuring error and achieve the best machine design. Finally, the results of the analytical error model were confirmed through a Monte Carlo analysis.

Keywords: micro-CMM, parallel manipulator, micro-measurement, covariance matrix, error model, Monte Carlo simulation.

1 Introduction

The machining, assembly inspection and quality controlling of small objects such as micro-electro-mechanical systems (MEMS) require high positioning accuracy. During the past two decades great attention has been given to micrometrology to fill the gap between the ultrahigh precision measurements of nanometrology and macrometrology [1]. In this regard many micro coordinate measuring machines (micro-CMM) were introduced and intensively studied [2-4].

The fact that the errors are not cumulative and amplified is one of the major advantages of parallel CMMs over the traditional serial CMMs [5]. Nonetheless, the positioning accuracy of parallel mechanisms is usually limited by many other errors, some authors identified the errors affecting the precision of parallel mechanisms as follows [5-8]: manufacturing errors, assembly errors, errors resulting from distortion by force and heat, control system errors and actuators errors, calibration, and even mathematical models. However, the main disadvantage of parallel CMMs is the limited workspace [9-11], and the difficulty of their motion control due to singularity problems [5], [11]. Many researchers studied the singularity problem and workspace analysis of some planar parallel mechanisms [13], [14]. Previous studies showed the influence of joint manufacturing and assembly on the positioning error [5], [15]. Pierre [16] showed that the operation and the performance of the sensors significantly affect the precision of the manipulator. Hassan analysed the tolerance of the joints [17], Tian studied the assembly errors [9]. Tasi [18], Raghavan [19], Abderrahim and Whittaker [20] have studied the limitations of various modelling methods. The solution of the forward kinematic for various configurations has attracted the attention of many researchers [21-28]. The performance of micro-CMMs in terms of accuracy and precision is influenced by numerous error parameters that require effective error modelling methods [15], [29]. Moreover, the error models are of great importance in order to evaluate the machine and understand the effect of the different parameters. Forward solution for error analysis was also covered [30-32].

This paper presents a micro-CMM based on parallel mechanism [33], [34]. Its workspace was analysed, and details of the measuring model are reported. An error model of the mechanism given the covariance matrix theory was established, and the effect of geometrical errors on the position were analysed.

2 Structure and theory

2.1 Machine design & Structure

The micro-CMM designed in this research consists of an upper equilateral triangular frame and a lower equilateral triangular moving platform connected to the upper frame with three extendable legs. Each leg contains a prismatic joint, the upper/lower ends of the legs are connected to the frame/platform (at points f_i / p_i)

with spherical joints. Moreover, laser interferometers are installed on the legs in order to acquire accurate measurement of the length of the legs. The lower platform can only move with respect to the upper frame. The movement of the platform is controlled by three linear motors attached to the upper frame. An isometric view and a top view of the machine are shown in Fig. 1.

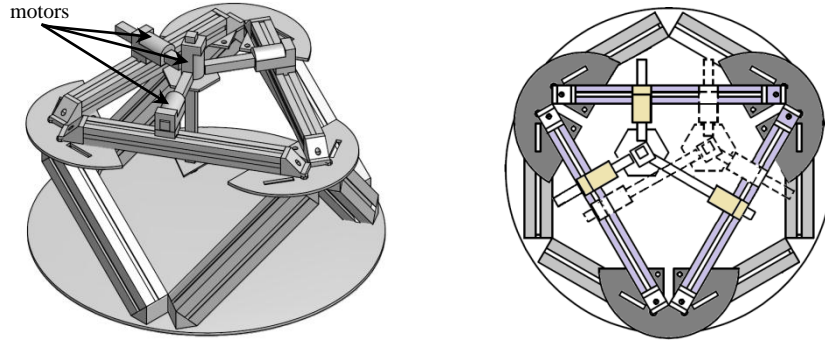


Fig. 1. Micro-CMM design. Isometric (left) and top view (right).

In Oiwa's design [33], the workspace is very small because of the rotational joints' limitation. Our arrangement provides significant advantage by using spherical joints. The spherical joints represent three rotational degrees of freedom (3-DOF). In this arrangement the use of spherical joints ensures that a very large workspace is achieved. However, the movement of the platform is restricted to always be parallel to the upper frame. The sacrifice of the rotational movement of the moving platform around the axes is beneficial for solving the kinematics model. Fig. 2 shows a schematic drawing of the micro-CMM machine.

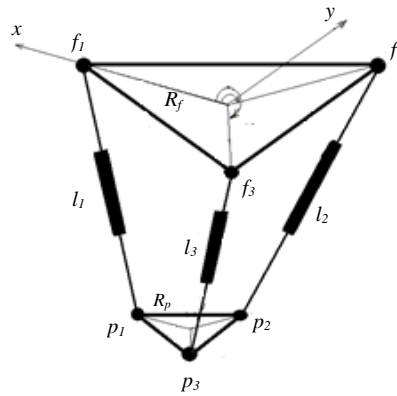


Fig. 2. Schematic drawing of the micro-CMM machine.

2.2 Coordinate system

The coordinate system is shown in Fig. 3. The origin $O_f(0,0,0)$ is placed at the centre of the upper frame. The x -axis equally divides the angle at point f_1 and the z -axis is perpendicular to the frame plane.

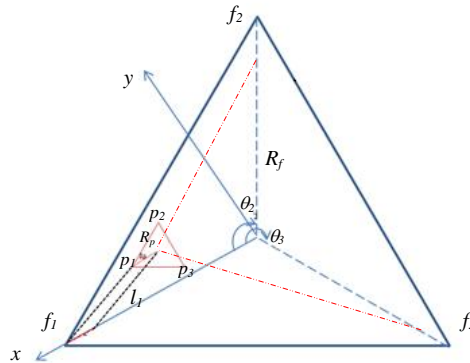


Fig. 3. The coordinate system.

The geometrical parameters are as follows:

- R_f : the distance between point f_i and the origin O_f , $R_f = 288$ mm
- R_p : the distance between point f_i and the origin O_f , $R_p = 57.5$ mm

- θ_i : the angle point f_i makes with the x -axis, $\theta_1 = 0^\circ$, $\theta_2 = 120^\circ$, $\theta_3 = 240^\circ$
- l_{min}, l_{max} : the maximum and minimum extensions of the legs, $l_{min} = 300$ mm, $l_{max} = 550$ mm

3 Development of the kinematic model

Because of using spherical joints, the movement of the legs can be expressed by the equation of a sphere. Let's assume that the central point of the moving platform (x,y,z) is the point of intersection of three spheres, and thus, point f_i must be shifted towards the point of origin O_f by $(f_i - p_i)$ where:

$$p_i = [R_p \cos \theta_i \quad R_p \sin \theta_i \quad z]^T \quad (1)$$

$$f_i = [R_f \cos \theta_i \quad R_f \sin \theta_i \quad 0]^T \quad (2)$$

Then the equation of movement of the legs can be written as follows:

$$l_1^2 = [x - (R_f - R_p) \cos \theta_1]^2 + [y - (R_f - R_p) \sin \theta_1]^2 + [z]^2 \quad (3)$$

$$l_2^2 = [x - (R_f - R_p) \cos \theta_2]^2 + [y - (R_f - R_p) \sin \theta_2]^2 + [z]^2 \quad (4)$$

$$l_3^2 = [x - (R_f - R_p) \cos \theta_3]^2 + [y - (R_f - R_p) \sin \theta_3]^2 + [z]^2 \quad (5)$$

Where:

(x,y,z) : the probe location
 l_1, l_2 and l_3 : the leg lengths.

The probe location can be found by solving eq's (3), (4) and (5). This yields explicit expressions for the x , y and z coordinates of the centre point

$$x = \frac{2l_1^2 + l_2^2 + l_3^2}{4(R_f - R_p)(\cos \theta_1 - \cos \theta_2)} - \frac{(R_f - R_p)(\cos \theta_2^2 - 1)}{2(\cos \theta_1 - \cos \theta_2)} \quad (6)$$

$$y = \frac{l_2^2 - l_3^2}{2(R_f - R_p)(\sin \theta_2 - \sin \theta_3)} - \frac{(R_f - R_p)(\sin \theta_2^2 - \sin \theta_3^2)}{2(\sin \theta_2 - \sin \theta_3)} \quad (7)$$

$$z = \sqrt{l_2^2 - [X + (R_f - R_p) \cos \theta_2]^2 - [Y + (R_f - R_p) \sin \theta_2]^2} \quad (8)$$

4 Analysis of the work space

The reachable workspace of a parallel manipulator is defined as all the positions within the region of the Cartesian space that can be reached by the tip of the probe which is attached to the central point of the platform. The workspace can be determined using the previously described model. The boundary surfaces of the workspace are calculated taking into account all the geometrical limitations and the movement range of the prismatic joints of the legs (maximum extension l_{max} and the minimum extension l_{min}).

Fig. 4 shows a 3D plot of the reachable work space. The processes of constructing the workspace can be summarized as follows:

- Set boundary conditions ($y_{max} = (R_f - x) \tan(30)$, $y_{min} = -(R_f - x) \tan(30)$, $x_{max} = R_f$, $x_{min} = -R_f/2$)
- Set one leg $l_i = l_{min}$, increase the other two legs by δl from l_{min} to l_{max}
- Solve the position components (x,y,z) for the outer surfaces S_{out-li} .
- Set one leg $l_i = l_{max}$, increase the other two legs by δl from l_{min} to l_{max} .
- Solve the position components (x,y,z) for the inner surfaces S_{in-li} .
- Repeat for each leg.
- Solve for the side surfaces S_1, S_2, S_3 .
 - S_1 : $y = (R_f - x) \tan(30)$, with x in the range $(x_{min} \leq x \leq x_{max})$
 - S_2 : $y = -(R_f - x) \tan(30)$, with x in the range $(x_{min} \leq x \leq x_{max})$
 - S_3 : $x = x_{max}$ and y in the range $(y_{min} \leq y \leq y_{max})$

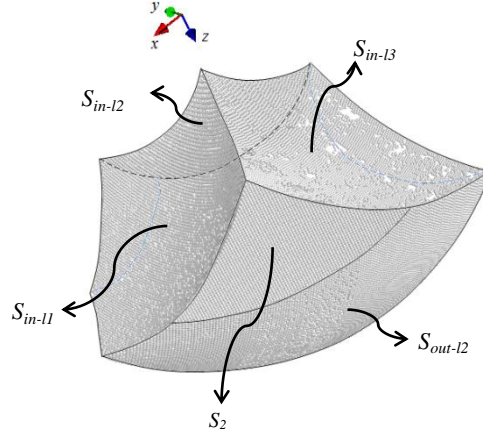


Fig. 4. 3D plot of the reachable workspace.

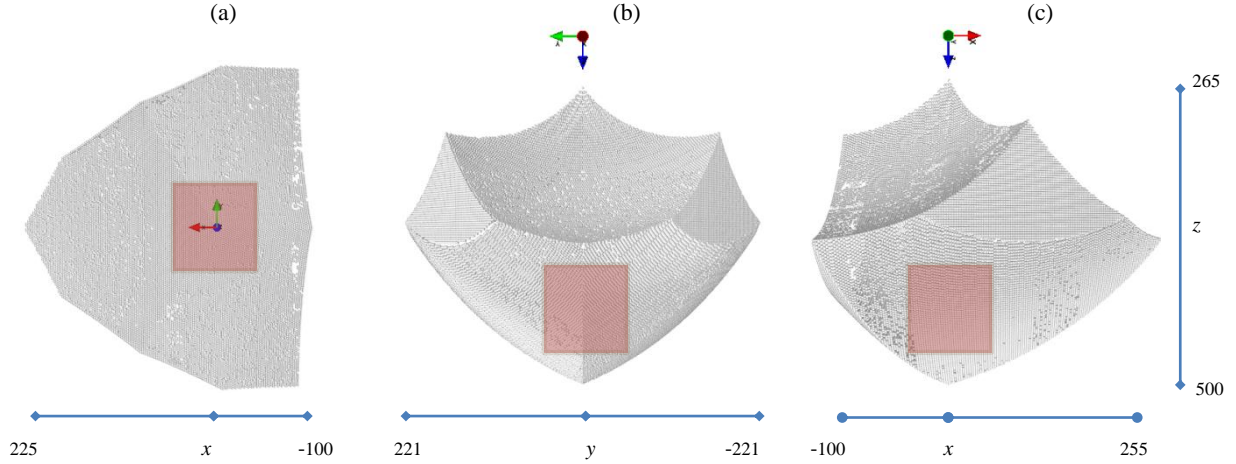


Fig. 5. The reachable workspace of the micro-CMM. (a) top view; (b) front view; (c) side view.

The results of workspace calculations illustrated in Fig. 4 and Fig. 5 show that: (1) The workspace is formed by surfaces cascaded together. (2) The workspace is symmetric about the xz plane. (3) The workspace range in xy plane vanishes at z_{min} where $l_1=l_2=l_3=l_{min}$, and reaches its maximum range when two legs are maximum and the third is minimum, then the range decreases as z increases and vanishes at $z > 500$ mm when $l_1=l_2=l_3=l_{max}$. The red cube in the workspace represent the work envelope (100x100x100) mm.

5 Modelling of the error

5.1 Analytical error model

Suggesting an error model for the proposed machine is of great importance in order to evaluate the structure and understand the effect of the different parameters on its accuracy. The derivation of the covariance matrix is well known and can be found in in refs. [35], [36]. For more clarification the details of the derivation will be given here:

If $F(x)$ is a vector valued function, the form of the first order Taylor series expansion can be given by:

$$F(x) = F(\bar{x}) + J(\bar{x}) \cdot (x - \bar{x}) + (\varepsilon \|x - \bar{x}\|^2) \quad (9)$$

Where: $J(x)$ is the Jacobian matrix of $F(x)$, and ε is the error term, \bar{x} is the average of all x samples.

Let's assume that the last term is small enough to be neglected. Then the previous equation can be rewritten as:

$$F(x) - F(\bar{x}) = J(\bar{x}) \bullet (x - \bar{x}) \quad (10)$$

The formula for computing the covariance is:

$$A_F = \frac{1}{n-1} (F(x) - F(\bar{x})) \bullet (F(x) - F(\bar{x})) \quad (11)$$

Replacing the dot product by the transpose of two matrices $A \bullet B = A^T B$, we get:

$$\Lambda_F = \frac{1}{n-1} (F(x) - F(\bar{x}))^T (F(x) - F(\bar{x})) \quad (12)$$

Replace eq. (10) . in eq. (11) to get:

$$\Lambda_F = \frac{1}{n-1} (J(\bar{x}) \bullet (x - \bar{x}))^T (J(\bar{x}) \bullet (x - \bar{x})) \quad (13)$$

Remember, the dot product is commutative $A \bullet B = B \bullet A$, and $(AB)^T = A^T B^T$, then Λ_F can be rewritten as:

$$\Lambda_F = \frac{1}{n-1} J(\bar{x}) (x - \bar{x})^T (x - \bar{x}) (J(\bar{x}))^T \quad (14)$$

Since the covariance matrix of x is:

$$\Lambda_x = \frac{1}{n-1} (x - \bar{x})^T (x - \bar{x}) \quad (15)$$

Then the covariance matrix can be written as:

$$\Lambda_F = J(\bar{x}) \Lambda_x J(\bar{x})^T \quad (16)$$

The last equation is very useful to determine the covariance matrix using the input covariance and the Jacobian of the process function.

Assuming that only mechanical errors among these errors have an influence on the positioning accuracy. The geometry of each stage (or leg) can be expressed by five geometrical parameters, which are the leg lengths l_i and the position of each spherical joint f_i and p_i in the Cartesian coordinate system. Therefore in total 15 parameters will be investigated. Thus, eq's (6), (7), and (8) must be rewritten as:

$$x = \frac{(l_2^2 - l_3^2) - (x_2^2 - x_3^2) - (y_2^2 - y_3^2)}{2(x_3 - x_2)} - Y \frac{(y_3 - y_2)}{(x_3 - x_2)} \quad (17)$$

$$y = \frac{(l_1^2 - l_2^2) - (x_1^2 - x_2^2) - (y_1^2 - y_2^2) - \frac{(x_2 - x_1)}{(x_3 - x_2)} [(l_2^2 - l_3^2) + (x_3^2 - x_2^2) - (y_3^2 - y_2^2)]}{2 \left[(y_1 - y_2) - \frac{(x_2 - x_1)}{(x_3 - x_2)} (y_3 - y_2) \right]} \quad (18)$$

$$z = \sqrt{l_2^2 - (X - x_2)^2 - (Y - y_2)^2} \quad (19)$$

where:

$$x_i = R_{fi} \cos(\theta_{fi}) - R_{pi} \cos(\theta_{pi}); \quad y_i = R_{fi} \sin(\theta_{fi}) - R_{pi} \sin(\theta_{pi}); \quad i = 1,2,3$$

A full size Jacobian matrix is used in carrying out error analysis, the Jacobian needed will be 3x15 matrix as follows:

$$J = \begin{bmatrix} \frac{\partial x}{\partial l_1} & \frac{\partial x}{\partial l_2} & \frac{\partial x}{\partial l_3} & \frac{\partial x}{\partial R_{p1}} & \frac{\partial x}{\partial R_{p2}} & \frac{\partial x}{\partial R_{p3}} & \frac{\partial x}{\partial R_{f1}} & \frac{\partial x}{\partial R_{f2}} & \frac{\partial x}{\partial R_{f3}} & \frac{\partial x}{\partial \theta_{p1}} & \frac{\partial x}{\partial \theta_{p2}} & \frac{\partial x}{\partial \theta_{p3}} & \frac{\partial x}{\partial \theta_{f1}} & \frac{\partial x}{\partial \theta_{f2}} & \frac{\partial x}{\partial \theta_{f3}} \\ \frac{\partial y}{\partial l_1} & \frac{\partial y}{\partial l_2} & \frac{\partial y}{\partial l_3} & \frac{\partial y}{\partial R_{p1}} & \frac{\partial y}{\partial R_{p2}} & \frac{\partial y}{\partial R_{p3}} & \frac{\partial y}{\partial R_{f1}} & \frac{\partial y}{\partial R_{f2}} & \frac{\partial y}{\partial R_{f3}} & \frac{\partial y}{\partial \theta_{p1}} & \frac{\partial y}{\partial \theta_{p2}} & \frac{\partial y}{\partial \theta_{p3}} & \frac{\partial y}{\partial \theta_{f1}} & \frac{\partial y}{\partial \theta_{f2}} & \frac{\partial y}{\partial \theta_{f3}} \\ \frac{\partial z}{\partial l_1} & \frac{\partial z}{\partial l_2} & \frac{\partial z}{\partial l_3} & \frac{\partial z}{\partial R_{p1}} & \frac{\partial z}{\partial R_{p2}} & \frac{\partial z}{\partial R_{p3}} & \frac{\partial z}{\partial R_{f1}} & \frac{\partial z}{\partial R_{f2}} & \frac{\partial z}{\partial R_{f3}} & \frac{\partial z}{\partial \theta_{p1}} & \frac{\partial z}{\partial \theta_{p2}} & \frac{\partial z}{\partial \theta_{p3}} & \frac{\partial z}{\partial \theta_{f1}} & \frac{\partial z}{\partial \theta_{f2}} & \frac{\partial z}{\partial \theta_{f3}} \end{bmatrix} \quad (20)$$

The related variances matrix is given by the following 15x15 diagonal matrix:

$$\Lambda_p = \begin{bmatrix} \sigma_{l_1}^2 & 0 & \dots & 0 \\ 0 & \sigma_{l_2}^2 & & \\ \vdots & & \ddots & \\ 0 & 0 & \dots & \sigma_{\theta_{f3}}^2 \end{bmatrix} \quad (21)$$

In the previous matrix the variance along the diagonal is given for $l_1, l_2, l_3, R_{p1}, R_{p2}, R_{p3}, R_{f1}, R_{f2}, R_{f3}, \theta_{p1}, \theta_{p2}, \theta_{p3}, \theta_{f1}, \theta_{f2}, \theta_{f3}$. Precision error values are mostly considered as three times the standard deviation value ($\varepsilon = 3\sigma$). Thus, the variance can be estimated by:

$$\sigma_p^2 = \left(\frac{\varepsilon_p}{3}\right)^2 \quad (22)$$

Where: σ_p^2 and ε_p are the variance and the error of the parameters, respectively.

5.2 Monte Carlo simulation

In Monte Carlo studies, random parameter values are generated from an allowed error range. A large number of runs are carried out, and the model is estimated for each run. Parameter values and standard errors are averaged over the samples.

The Monte Carlo simulations have been used as uncertainty evaluation for CMM's in Refs. [37-40]. This method was documented in an ISO document [41]. In this study simulations have been performed to examine the validity of analytical error model. Computer software developed in Python was used to overcome the amount of work needed for the simulation.

Several combinations of conditions have been chosen (I) at maximum legs extensions, (II) minimum extension of the legs. The number of Monte Carlo iterations are $n = 50000$.

The following values of the parameters are used: $R_{b1}, R_{b2}, R_{b3} = 288 \pm 0.002$ mm; $R_{p1}, R_{p2}, R_{p3} = 57 \pm 0.002$ mm; $\theta_{p1}, \theta_{b1} = 0^\circ \pm 0.0005^\circ$, $\theta_{p2}, \theta_{b2} = 120^\circ \pm 0.0005^\circ$, $\theta_{p3}, \theta_{b3} = 240^\circ \pm 0.0005^\circ$; $l_1, l_2, l_3 = l \pm 0.001$ mm.

6 Results of the error model

The geometrical parameters are given as follows: $R_{f1}, R_{f2}, R_{f3} = 288$ mm, $R_{p1}, R_{p2}, R_{p3} = 57.5$ mm, $\theta_{p1}, \theta_{f1} = 0^\circ$, $\theta_{p2}, \theta_{f2} = 120^\circ$, $\theta_{p3}, \theta_{f3} = 240^\circ$, $l_{min} = 288$ mm, $l_{max} = 433$ mm.

The covariance matrix of measurement errors is found by the proposed analytical approach in eq. (16). The variance-covariance matrix consists of the variances of x , y and z along the main diagonal and the covariances between each pair of variables in the other matrix positions. The covariance between xy , xz and yz is very small and can be neglected, hence x , y and z can be assumed uncorrelated.

The results of the Monte Carlo simulation are represented in the form of a typical histogram in Fig. 6. The histograms are useful as an aid to understanding the nature of the data distribution.

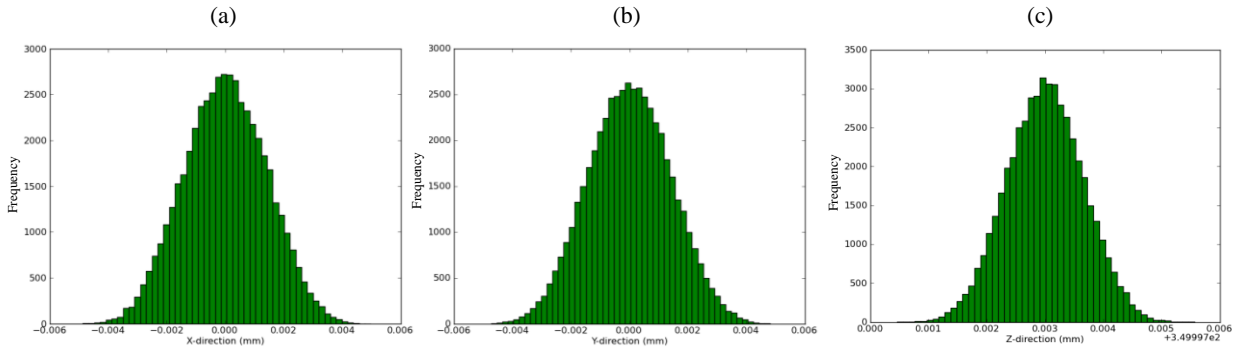


Fig. 6. Results of Monte Carlo simulation, (a) histogram of x , (b) histogram of y , (c) histogram of z .

From Fig. 6, the histogram plots for x , y and z indicate that the data are approximated well by a normal distribution, therefore it is reasonable to use the standard deviation as the distribution estimator.

Comparisons of simulated results with the analytical results in terms of standard deviations (σ) are tabulated in Table 1.

Table 1. Comparison of the simulation results with the analytical results:

| | $\varepsilon_{li} = \pm 0.001$; $\varepsilon_{R_{fi}}, \varepsilon_{R_{pi}} = \pm 0.002$; $\varepsilon_{\theta_{fi}}, \varepsilon_{\theta_{pi}} = \pm 0.0005^\circ$ | | | |
|------------------|---|-------------------------|---------------------|-------------------------|
| | $x=0; y=0; z=350$ | | $x=50; y=50; z=350$ | |
| | Theory (σ) | Simulation (σ) | Theory (σ) | Simulation (σ) |
| $x(\mu\text{m})$ | 0.811 | 0.702 | 0.760 | 0.658 |
| $y(\mu\text{m})$ | 0.811 | 0.702 | 0.918 | 0.796 |
| $z(\mu\text{m})$ | 0.361 | 0.313 | 0.355 | 0.309 |

6.1 Effect of structural errors on probe position

The following values of the mechanical errors were used in the error model: $\varepsilon R_{fi} = \pm 0.002$ mm, $\varepsilon R_{pi} = \pm 0.002$ mm, $\varepsilon l_i = \pm 0.001$ mm, $\varepsilon \theta_{fi} = \pm 0.0005^\circ$ and $\varepsilon \theta_{pi} = \pm 0.0005^\circ$. Fig. 7 shows the σ_x , σ_y , and σ_z estimated using the analytical model. The three continuous lines represent σ_x , σ_y and σ_z with an error of $\varepsilon l_i = \pm 1 \mu\text{m}$, the dashed line represents σ_z when the error in the legs is $\pm 2 \mu\text{m}$.

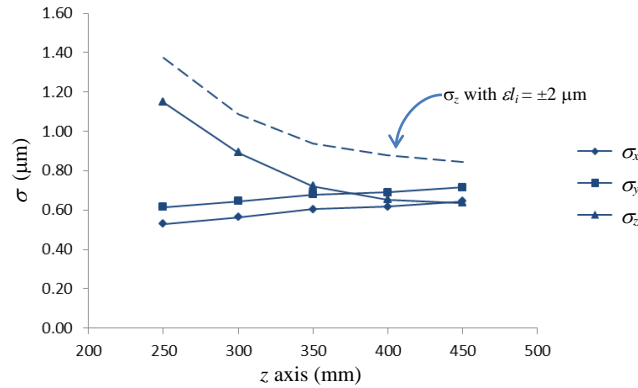


Fig. 7. Error estimation along z axis.

From Fig. 7, σ_z decreases dramatically as the moving platform translates away from the point of origin in the z direction, the σ_z starts to decrease very slowly when z value is greater than 350 mm, in other words, the probe is 350 mm below the upper frame. The work envelope in the z direction is in the range (350 – 450). Moreover, Fig. 8 shows the xy plane at z = 400.

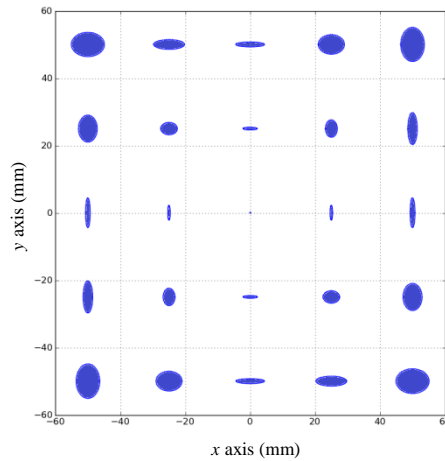


Fig. 8. The xy plane at z = 400, with σ_x , σ_y magnified 10^4 times.

From Fig. 8, it is clear that the maximum error values in x and y directions are in the corners of the xy plane, however, the error decreases as the probe moves closer to the origin, and reaches minimum value at $x=y=0$. The work envelope in both directions x and y is in the range ($-50 \leq x, y \leq 50$).

7 Concluding remarks

A micro-CMM offering very large workspace was proposed, the workspace was analysed, a kinematic model was derived, and the error was modelled. The work envelope with a submicron estimated error was ($-50 \leq x, y \leq 50$) in x and y directions, and ($350 \leq z \leq 450$) in z direction.

It can be observed from the results that the analytical error model is effective with an input error of 0.5 to 2 μm . This was verified using Monte Carlo simulation results. In this study the error values are chosen arbitrary, more accurate geometrical errors can be estimated using the finite element method. The l_i has the most significant contribution to the error is z scale, while in x and y directions angle θ_i is responsible for the most significant effect on the accuracy. The positioning accuracy of the micro-CMM is also limited by many other error sources. However, geometrical errors can be minimized by improving the precision of manufacture and assembly.

References

1. P McKeown, "Nanotechnology-Special article," in *Nano-metrology in Precision Engineering*, Hong Kong, 1998, pp. 5-55.
2. Fan Kuang-Chao, Fei Yetai, and Yu Xiaofen, "Development of a micro-CMM," in *International Manufacturing Leaders Forum on "Global Competitive Manufacturing"*, Adelaide, Australia, 2005, pp. 1-7.
3. F Gao, W M Lin, and X C Zhao, "New kinematic structures for 2-, 3-, 4-, and 5-DOF parallel manipulator designs," *Mechanism and Machine Theory*, vol. 37, pp. 1395–1411, 2002.
4. X J Liu, J S Wang, and G Pritschow, "A new family of spatial 3-DOF fully-parallel manipulators with high rotational capability," *Mechanism and Machine Theory*, vol. 40, pp. 475–494, 2005.
5. Cheng Gang, Shi-rong Ge, and Yong Wang, "Error analysis of three degree-of-freedom changeable parallel measuring mechanism," *Journal of China University of Mining & Technology*, vol. 17, no. 1, pp. 101-104, 2007.
6. Che R S Meng Z, "Error model and error compensation of six-freedom-degree parallel mechanism CMM," *Journal of Harbin Institute of Technology*, vol. 36, no. 3, pp. 317–320, 2004.
7. Ma Li, Rong Weibin, Sun Lining, and Li Zheng, "Error compensation for a parallel robot using back propagation neural networks," in *International Conference on Robotics and Biomimetics*, Kunming, 2006, pp. 1658-1663.
8. Meng Z, Che R.S, Huang Q.C, and Yu Z.J, "The direct-error-compensation method of measuring the error of a six-freedom-degree parallel mechanism CMM," *Journal of Materials Processing Technology*, vol. 129, pp. 574–578, 2002.
9. K.H Hunt, "Structural kinematics of in parallel-actuated robot arms," *ASME Journal of Mechanisms, Transmissions, and Automation in Design*, vol. 105, pp. 705–712, 1983.
10. R Clavel and Delta, "A fast robot with parallel geometry," in *International Symposium on Industrial Robots*, Switzerland, 1988, pp. 91–100.
11. John J Craig, *Introduction to Robotics: Mechanics and Control*, 2nd ed. New York, USA: Addison and Wesley, 1989.
12. K Sugimoto, J Duffy, and K.H Hunt, "Special configurations of spatial mechanisms and robot arms," *Mechanism and Machine Theory*, vol. 17, no. 2, pp. 119–132, 1982.
13. Z M Ji, "Study of planar three-degree-of-freedom 2-RRR parallel manipulator," *Mechanism and Machine Theory*, vol. 38, pp. 409-416, 2003.
14. X J Liu, J S Wang, and G Pritschow, "Kinematics, singularity and workspace of planar 5R symmetrical parallel mechanisms.," *Mechanism and Machine Theory*, vol. 41, pp. 145–169, 2006.
15. Rui YAO, Xiaoqiang TANG, and Tiemin LI, "Error Analysis and Distribution of 6-SPS and 6-PSS Reconfigurable," *Tsinghua Science and Technology*, vol. 15, no. 5, pp. 547-554, October 2010.
16. R Pierre, A Nicolas, and M Philippe, "Kinematic calibration of parallel mechanisms: a novel approach using legs observation," *IEEE Transactions on Robotics*, vol. 4, pp. 529–538, 2005.
17. H Mahir and N Leila, "Design modification of parallel manipulators for optimum fault tolerance to joint jam," *Mechanism and Machine Theory*, vol. 40, pp. 559–577, 2005.
18. Lung-wen Tsai, *Robot Analysis-The Mechanics of Serial and Parallel Manipulators*. New York, USA: Wiley, 1999.
19. M Raghavan, "The Stewart platform of general geometry has 40 configurations," *ASME Journal of Mechanical Design*, vol. 115, pp. 277–82, 1993.
20. M Abderrahim and AR Whittaker, "Kinematic model identification of industrial manipulators," *Journal of Robotic Computer Integrated*, vol. 16, pp. 1–8, 2000.
21. AK Dhingra, AN Almadi, and D Kohli, "Closed-form displacement analysis of 8, 9 and 10-Link Mechanisms," *Mechanism and Machine Theory*, vol. 35, pp. 821-850, 2000.
22. Shi Xiaolun and RG Fenton, "A complete and general solution to the forward kinematics problem of platform-type robotic manipulators," *IEEE*, pp. 3055–3062, 1994.
23. Olivier Didrit, Micheal Petitot, and Eric Walter, "Guaranteed solution of direct kinematic problems for general configurations of parallel manipulators," *IEEE Transactions on Robotics and Automation*, vol. 14, no. 2, pp. 259–266, 1998.
24. Zhang, Chang-de and Song Shin-Min, "Forward kinematics of a class of parallel (Stewart) platform with closed-form solutions," in *IEEE International Conference on Robotics and Automation*, Sacramento, California, 1991, pp. 2676–2681.
25. Prabjot Nanua, KJ Waldron, and V Murthy, "Direct kinematic Solution of a Stewart platform," *IEEE Transactions on Robotics and Automation*, vol. 6, no. 4, pp. 431–7, 1990.
26. SV Sreenivasan, KJ Waldron, and P Nanua, "Closed-form direct displacement analysis of a 6-6 Stewart platform," *Mechanism and Machine Theory*, vol. 29, no. 6, pp. 855–864, 1994.
27. M Griffis and J Duffy, "A forward displacement analysis of a class of Stewart platform," *Journal of Robotic Systems*, vol. 6, no. 6, pp. 703–720, 1989.
28. W Lin, M Griffis, and J Duffy, "Forward displacement analyses of the 4-4 Stewart platforms," *Trans ASME*, vol. 114, pp. 444–450, 1992.

29. Chunshen Lin, Xiaoqiang Tang, and Liping Wang, "Precision design of modular parallel kinematic machines," *Tool Engineering*, vol. 41, no. 8, pp. 38-42, 2007.
30. Wang Jian and Masory Oren, "On the accuracy of a stewart platform—Part I: The effect of manufacturing tolerances," in *IEEE International Conference on Robotics and Automation Los Alamitos*, Atlanta, GA, USA, 1993, pp. 114–20.
31. Gong Chunhe, Yuan Jingxia, and Ni Jun, "Nongeometric error identification and compensation for robotic system by inverse calibration," *International Journal of Machine Tools and Manufacture*, vol. 40, pp. 2119–2137, 2000.
32. AJ Patel and Kornel F Ehmman, "Calibration of a hexapod machine tool using a redundant leg," *International Journal of Machine Tools and Manufacture*, vol. 40, pp. 489–512, 2000.
33. T Oiwa, "New coordinate measuring machine featuring a parallel mechanism," *International Journal of the Japan Society for Precision Engineering*, vol. 31, no. 3, pp. 232-233, 1997.
34. Hanqi Zhuang and Yingl Wang, "A coordinate measuring machine with parallel mechanisms," in *IEEE Int. ConJ: on Robotics and Automation*, Albuquerque, New Mexico, 1997, pp. 3256-3261.
35. Zhixiang Zhao and F. G Perey, "The Covariance Matrix of Derived Quantities and their Combination," Oak Ridg National Laboratory, Beijing, China, Technical report ORNL/TM-12106, 1992.
36. J. C Clarke, "Modelling uncertainty: A primer," Department of Engineering, Oxford University, Oxford, UK, Technical report 1998.
37. P.B Dhanish and J Mathew, "Effect of CMM point coordinate uncertainty on uncertainties in determination of circular features," *Measurement*, vol. 39, pp. 522-531, 2006.
38. B.W.J.J.A Van Dorp, H Haitjema, and F.L.M Delbre, "A virtual CMM using Monte Carlo Methods based on Frequency Content of the Error Signal," in *SPIE*, Germany, Munich, 2001, pp. 158-167.
39. M Brizard, M Megharfi, and C Verdier, "Absolute falling-ball viscometer: evaluation of measurement uncertainty," *Metrologia*, vol. 42, pp. 298–303, 2005.
40. Suzanne J Canning, John C Ziegert, and Tony L Schm, "Coordinate metrology uncertainty using parallel kinematic techniques," *International Journal of Machine Tools & Manufacture*, vol. 47, pp. 658–665, 2007.
41. "Guide to the expression of uncertainty in measurement (GUM) — Supplement 1: Numerical methods for the propagation of distributions using a Monte Carlo Method," JCGM, (ISO), Draft JCGM 101:2008, 2008.